CCD photometry in modern astronomy [1]

K. Ohde and A. Hermann

Abstract: In this experiment we are determining the basic characteristics of the Tektronics TK1024 CCD-detector: linearity, dynamic range, sensitivity and noise properties. During the analysis of our measurements we familiarise ourselves with a number of data reduction techniques, such as bias correction. After that, we apply those techniques to perform photometric measurements on images of the globular cluster BS90 taken by the Hubble Space Telescope. From these measurements we compute a colour magnitude diagram and fit it manually with an isochrones. From those we determined it's age to be about 4.5Gyr, it's metallicity $Z = 1.5 \cdot 10^{-3}$ and a distance of 56kpc. At last we conduct our own observations of the galaxy M81 with the 70cm *King* telescope at the MPIA.

[1] Experiment F30, executed on 26.02.18, Tutor Leslie, special short evaluation

1 Introduction

In this experiment we familiarise ourselves with the properties of a CCD, a charged coupled device, and its uses in the field of astronomy. In order to do that, we first analyse the properties of the KING telescope at the MPIA and then use photometric techniques to analyse the images of the BS90 globular cluster observed by the Hubble space telescope. At the end we make our own observations with KING.

2 Theoretical background

2.1 Detectors

We gain information of the universe by analysing electromagnetic waves coming from space with typical radiation fluxes of an intensity of $10^{-29} W m^{-2} Hz^{-1} = 1 mJy$. Therefore the instrumentation must be able to detect signals precisely. The main advantages are: high sensitivity and dynamical range, linearity over almost the entire dynamical range, large spectral range and direct availability for further computer-aided data analysis[1].
The detection is based on a two-dimensional array of pixels, that are light-sensitive metal oxide semiconductor capacitors (MOS) on a silicon substrate. The resulting signal can be amplified and converted to a digital signal by an analogue digital converter (ADU).

2.1.1 Observations

As in the former section mentioned linearity is one advantage of the CCD detector. Linearity means, that an increase in the measured detector signal is proportional to an increase in the incoming photon flux. Since the detector is not able to derive the exact number of photons, in case the saturation level is reached, it is important to consider the integration time of the objects to observe. In general the integration time is indirect proportional to the strength of the source. Apart from that "dead" pixels and cosmics in the detector signal have to be considered. Both artefacts can be eliminated by taking several exposures of the object while moving the telescope slightly. Finally one is able to remove these values by aligning the frames and determining the median of each pixel.

2.1.2 Data Reduction

Due to imperfections in the production of the detector, there are small scale variations and large scale gradients in the sensitivity so that the intensity over the detector area is not constant. The variations in the sensitivity can be eliminated by a flat-field correction. Therefore several pictures of a flat surface with homogeneous emission are taken. Another preparation concerns the bias. This is a small constant value which is artificially added to the image to prevent negative values from bad pixels during the readout process. It is also added to a small overscan region which has no further physical meaning, or information. Another small error of any measurement comes from the dark current, which is a combination of thermal radiation and cosmic rays. Its distribution is random and thus statistical. To keep it small, we cool the CCD with liquid nitrogen to a temperature of $-196°C$. The temperature dependency of the dark current I is given by:

$$I(T) = const.\ T^{\frac{3}{2}} e^{-\frac{E_g}{2k_B T}} \tag{1}$$

Where E_g is the band gap of the semiconductor and k_B is the boltzmann constant.

2.2 Basic principles of photometry

To be able to analyse the properties of an astronomical object, we need to know its luminosity. However, as the distance to the observed object is unknown in most cases, it is not directly possible to specify it. The problem is aggravated by the circumstance that every instrument exhibits a different

sensitivity to the light of the star. Thus it is necessary to introduce different magnitude scales: The *instrumental magnitude* is a relative unit, allowing the comparison of different sources in one observation. The measured counts are converted to a logarithmic scale with arbitrary zero point:

$$m_{inst.} = zero\ point - 2.5 log\ counts \tag{2}$$

With the help of standard stars with known magnitudes the instrumental magnitude can be converted to the apparent magnitude. The *apparent magnitude* m is the brightness of the star as perceived from Earth. Finally, the *absolute magnitude* M is defined as the apparent magnitude the stars would have if they were a distance of 10pc away. With that, we can estimate the distance d of a star using the relationship:

$$d = 10^{(m-M+5)/5}\ [pc] \tag{3}$$

2.3 The Hertzsprung-Russel-Diagram (HRD) and the colour magnitude diagram (CMD)

The HRD allows the classification of stars in terms of their age, luminosity and mass. Therefore the relation between the effective temperature and the luminosity are subject of the HRD. The correlation between these two evokes a main sequence, where the majority of the stars is located. Since the absolute magnitudes and luminosities of many stars are unknown, the CMD is used by observational astronomy instead. In this case the apparent magnitude m is plotted over the colour index, that is related to the effective temperature. These values can be gained through observations with two filters. Since one can draw important conclusions with the CMD as one could with the HRD, we used the CMD for analysis in our experiment.

2.4 The gain and noise properties

The number of incoming electrons per pixel N_e is due to Poisson statistics: $N_e = \sigma_e^2$ (9). The number of excited electrons per unit of the analogue digital converter (ADU) is the gain κ. This value leads to the connection of the final signal $N_{e,d}$ in the ADU to the original number N_e with:

$$N_e = \frac{\kappa}{\eta} Ne, d \tag{4}$$

where η is the quantum efficiency of the detector and we receive:

$$\sigma_{e,d}^2 = \frac{\eta}{\kappa} N_{e,d} \tag{5}$$

Apart from the photon noise the read-out noise of the gate amplifier σ_R and the Pixel-Response-Non-Uniformity noise σ_{PRNU} exist. The last one is caused by the difference of the quantum efficiency of the pixels. The PRNU noise increases linearly with the signal level:
$\sigma_{PRNU,e} = N_e f_{PRNU}$ while $f_{PRNU} \approx 0,01$. Finally the total noise is given by:

$$\sigma_{tot,d}^2 = \sigma_{e,d}^2 + \sigma_{R,d}^2 + \sigma_{PRNU,d}^2 \tag{6}$$

The PRNU noise is directly proportional to the signal level. So in the experiment we subtract the two flat frames with the same signal level. The only source of noise left in this difference image, $\sigma_{diff,d}$, is then a combination of read-out noise and photon noise:

$$\sigma_{diff,d} = \sqrt{2} \cdot \sqrt{\sigma_{R,d}^2 + \sigma_{e,d}^2} \tag{7}$$

Combining equation (5) and (7)(assuming $\eta = 1$) we get:

$$\sigma_{diff,d}^2 = 2(\sigma_{R,d}^2 + \frac{N_{e,d}}{\kappa}) \tag{8}$$

3 Execution and evaluation

3.1 Layout of the experiment

The experiment takes place in the telescope dome of the Königstuhl where the 70cm KING telescope is located. It has exchangeable filters and uses a Tektronics TK1024 CCD-detector, which is located in a cryostat connected to a vacuum pump, where we cool it with liquid nitrogen to $\sim 115K$. The pressure has to be around $p = 10^{-6}mbar$ to avoid heat conduction and water vapour to freeze out on the camera. All information received by the detector will be read out by a pulse generator amplifier and an ADU. The telescope has parallactic mounting so that we can use the Cassegrain mode. The CCD detector contains 2048×2048 pixels of $15microns$. The pixel scale of the camera is $0.55"/pixel$. The pixels are saturated at about 60000 counts at a gain value of 5. The data is stored at a computer. For the data reduction, we used the IRAF software system.

3.2 Properties of the dark current

Before actually starting working with the telescope, a few preparations are needed to be done. First of all we cool down the CCD with liquid nitrogen. This is necessary to reduce the dark current which decreases the dynamical range and deteriorates the sensitivity of the system. As we cooled it down, we recorded 200 dark images with a binning factor of 2, a gain factor of 5 and an exposure time of 30s, as well as the current temperature of the CCD. We then extracted the median value of the overscan region to determine the bias of each picture and subtracted it from each picture individually. This is done, because the bias is artificially superposed over each picture and can be slightly different for each take. Hereafter we extracted the median values of the dark current from the bias corrected takes and graphed them against the temperature of the CCD(see fig.1) to confirm the relationship shown in equation (1) and to determine the band gap of the detector chip.

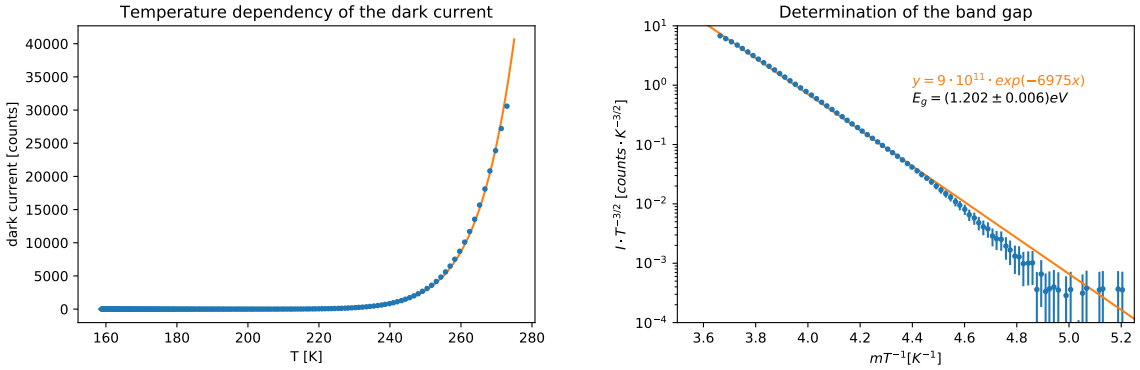

(a) Dark current vs temperature

(b) Plot to determine E_g

Figure 1: Band gap determination from the temperature dependant dark current

Looking at the median bias values from two pictures, one from the start and one from the end of the measurement we can see that the median bias value dropped from 1437 ± 2 ($\sim 0°$C) to 1346 ± 1 ($\sim -114°$C), which confirms that one should subtract the bias individually from each picture.

From the fit we get the band gap

$$E_g = (1.202 \pm 0.006)eV \tag{9}$$

Which deviates by more than 10σ from the literature value $E_{g,SI} = 1.15eV$ for silicon. One explanation for that could be, that the band gap itself is slightly temperature dependant(this would also explain the slight deviation of the measurements from the fit at higher temperatures). Another explanation would be, that the detector chip doesn't only consist of silicon, either because it was intentionally doped, or due to unintentional errors in it's lattice.

3.3 Flat-field correction

In the next step, we took 5 dome flat-fields for each of the three filters R, V and I, with different integration times. This is done by pointing the telescope at a uniformly illuminated white cloth and taking pictures(with the blinds taken off). We need different integration times, since the filters have different transparency and because our lightsource isn't uniform over the whole spectrum. After that, we proceeded by bias-correcting the pictures, similarly to the darks in the last part, and then combining the flat-fields of each filter using IRAF and taking the median of the pictures. We take the median to ensure that extreme values of an individual take do not influence the result. Following that, we normalized the combined flat-fields, also called master flat-fields, by dividing them by their median value. The last step is crucial, as the master flat-field is needed to correct the small and large scale variations in the detected signal, caused by dust, pixel sensitivity, etc.. Therefore we need a map of scaling factors that all our measurements are then divided by. If the master flat-fields would not be normalized, it would greatly reduce the dynamical range of the system and we would lose data. This master flats also have to be done for each filter individually, since the filters themselves can also have variations on their surface. Small variations on the dome surface, such as bolts or small smudges on the cloth, however, do not influence the flat-field images, since the telescope is focused on objects several thousand parsecs away from us and can thus not resolve the objects inside the dome at all.

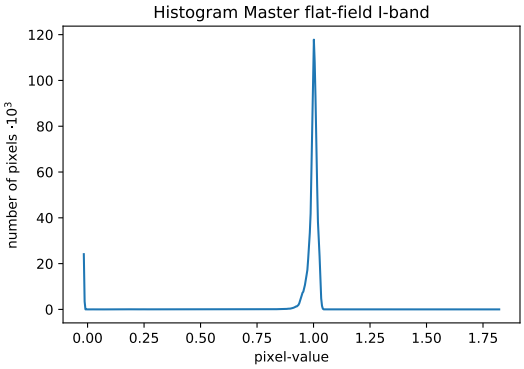

(a) I-band

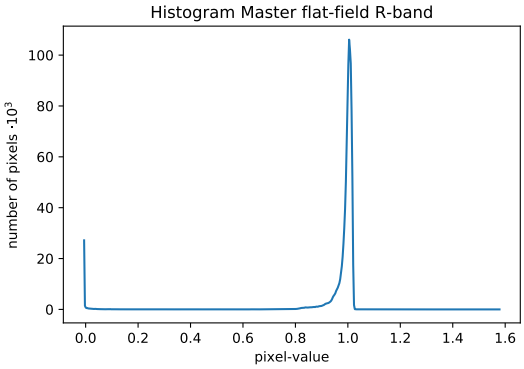

(b) R-band

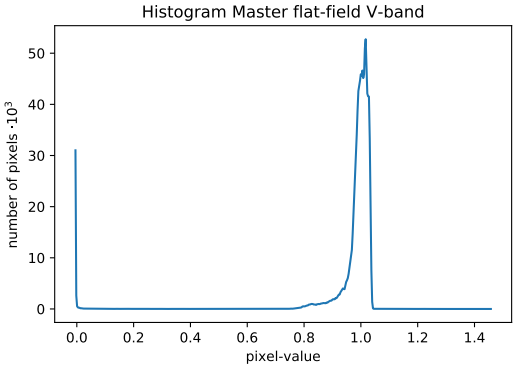

(c) V-band

Figure 2: Histograms of the master flat-fields

To ensure that our master flats are well made and to analyse them, we graphed their histogram. As you can see in figure 2, most of the pixels have, as expected, a value close to 1. However, around 30,000 pixels have a value close to 0. These are probably dead pixels. At last, we performed a flat-field correction on one of the flat-fields(see fig.3)

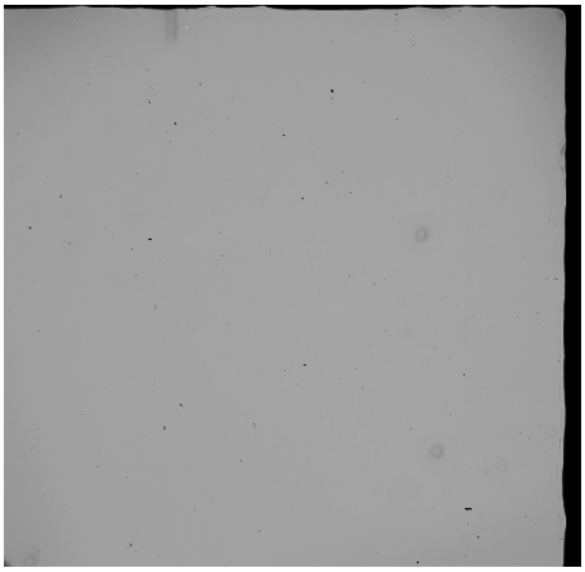

(a) Uncorrected flat-field R-band

(b) Corrected flat-field R-band

Figure 3: Example of a flat-field correction, performed on an individual flat-field image

3.4 Linearity and dynamic range

This time we use the same setup as in the previous section, but now we take about 15 flat-field images with the V filter with increasing integration time, to analyse the linearity of the CCD. To do that, we first had to bias-correct them and then perform a flat-field correction using the master flat from the previous section. From those corrected flat-fields we extract the integration time, as well as their median values and standard deviations and plot them in figure 4a. To analyse its linearity, we then fit the data with a linear function. The same procedure is then repeated for 22 images of the I filter(see fig.4b), which we will also use in the next section.

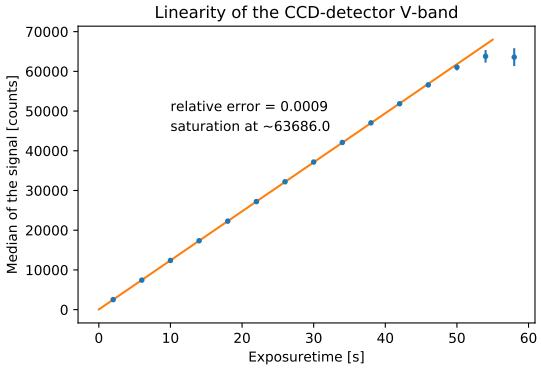

(a) V-band

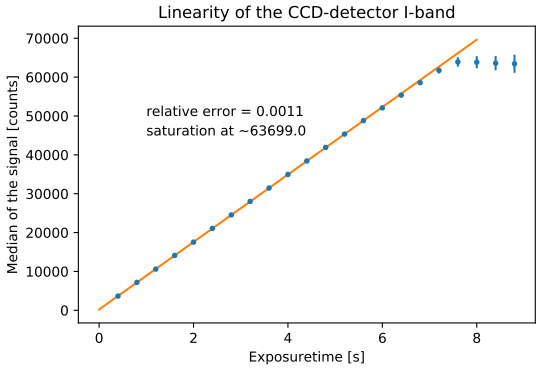

(b) I-band

Figure 4: Linearity of the CCD-detector

From the graphs we can see a very good linear relationship with a relative slope error of 0.09% and 0.11% respectively, up to about 60,000 counts, after which the saturation starts. The chip is saturated at about 63,700 counts.

3.5 Sensitivity of the detector and noise properties

In order to remove the effect of PRNU, we now take 22 pairs of flat-field images with different integration times in the I-band. We then extracted the read-out noise $\sigma_{R,d}$ from the overscan region, from

one pair of images with counts of $\sim 30,000$ counts. Following that, we chose a uniformly illuminated 200×200 pixel area and extracted the total noise $\sigma_{tot,d}$ and the median signal $N_{e,d}$ for the same pair of images in that area. We then subtracted the two images from another and then determined the noise of the difference image in the chosen region, $\sigma_{diff,d}$. Last but not least, we extracted the median signal $N_{e,d}$ of all image pairs inside the chosen region and made difference images of all image pairs. After which we extracted the noise of the difference images $\sigma_{diff,d}$ inside the region.

With the measurements taken, we first determine the photon, read-out and PRNU noise for one pair of images. To do that, we use equations (7) and (6) to determine the photon noise $\sigma_{e,d}$ and the PRNU noise $\sigma_{PRNU,d}$ respectively. Since we are using a pair of images, we take the mean of each standard deviation before taking it's root. With that, we get the results:

$$\begin{aligned} \sigma_{e,d} &= 10.7 \\ \sigma_{R,d} &= 5.0 \\ \sigma_{PRNU,d} &= 9.0 \end{aligned} \tag{10}$$

Which shows that the photon noise slightly dominates. This means, that the characteristic PRNU factor of our CCD is in the order of 10^{-3}, rather than 0.01. Next we plotted $\sigma^2_{diff,d}$ versus the median signal in the chosen region in figure 5. This plot shows us the signal dependency of the variance. As we can easily see, it does not follow the linear relationship as given by equation (8), instead, it seems to show three distinct linear relationships for different signal levels. The easiest to explain is the one near the saturation, as at that point all, non-broken, pixels simply have the maximum signal and thus no error. The other give us

$$\kappa = 940 \pm 60 \tag{11}$$

for signal levels below 30,000 and

$$\kappa = -3540 \pm 250 \tag{12}$$

for signal levels above 30,000. However, although this plot suggests that the signal to noise ration drastically increases after $\sim 30,000$ counts, it is misleading since at higher signal levels, PRNU noise dominates, but since PRNU can be eliminated by taking several pictures, it's not relevant for observations of luminous objects. Calculating the gain with equation (5) and using the data we acquired

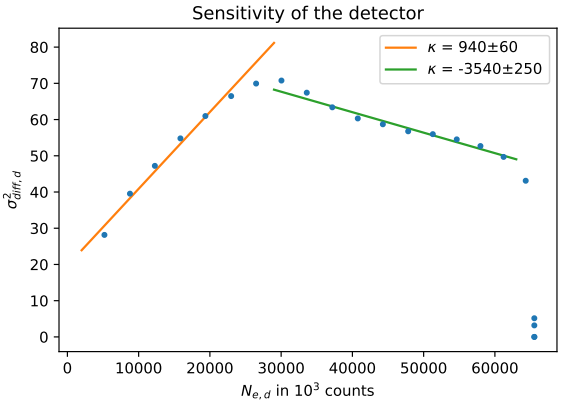

Figure 5: Sensitivity of the CCD-detector

from the one pair of images, we get

$$\kappa = 230.30 \pm 0.13 \tag{13}$$

The discrepancy can be explained with several factors. One would be, that, as mentioned above, that equation (8) is not representative for the actual relationship. The other would be, that the image we chose to take the data from had a mean close to 30,000 counts, meaning that it was in the transition between the first and the second value. And a last explanation would be, that in the first method, we averaged over several data points, while here we only used one. With that said, it's a rather good

ADU for observations with signal levels between 35,000 and 60,000 counts, due to the high absolute value of κ, as this means that in that region, the noise is almost a constant value.

3.6 Colour Magnitude Diagram

In this part we used archival images of the Hubble Space Telescope (HST) of the globular cluster BS90 to produce a color magnitude diagram that allowed us to estimate the distance, age, and metallicity of the cluster. To do that, we first had to get the zero-point magnitude. Which we did by comparing the counts of standard stars in the Hubble images with reference values of the apparent magnitude from an astronomical data base called SIMBAD. For this, we overplotted the V and I images from the catalogue "Cool evolved stars in SAGE-SMC and SAGE-LMC (Boyer+, 2011)" and selected 10 rather isolated stars. We then calculated the zero-point of each star using:

$$zeropoint = m_{CATALOGUE} + 2.5log_{10}(counts) \tag{14}$$

and then took the median of the values to get our final zero-points:

$$\begin{aligned} zeropoint_V &= 25.25 \pm 0.24 \\ zeropoint_I &= 25.10 \pm 0.16 \end{aligned} \tag{15}$$

After that we used starfinder, an IDL tool designed to perform PSF photometry that extracts a statistical PSF from the image and then tries to fit all stars in the image with that PSF. Using it involved following instructions, creating a PSF by selecting and clicking on stars that are just right and then waiting for the iterative process to be done. At the end of it, we got a list for each filter with stars that were detected. After that was done, we used a python script that cross-matched all the stars found in both filters and and subtracted the previously determined zero-points from the V and I magnitudes. Last but not least we plotted the results into a plot and fitted it with isochrones using the given script provided by the Osservatorio Astronomico di Padova, by adjusting the parameters shift, age and metallicity Z manually and comparing them to find the best fit. You can see the result in figure 6. Using the distance modulus m - M, given by the shift of the isochrones, and equation (3),

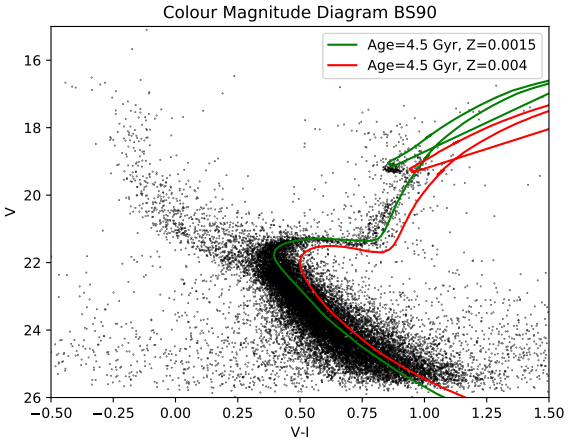

Figure 6: CMD plot with the best fitting isochrone(green) and the isochrone according to the literature(red).

we found the following values:

age [Gyr]	metallicity Z	distance modulus m - M [mag]	distance d [kpc]
4.5 ± 0.1	$(1.5 \pm 0.5) \cdot 10^{-3}$	18.75 ± 0.10	56.2 ± 2.6

Table 1: Properties of BS90 deduced from the isochrone fit

3.7 Scientific observations

In the end we had the opportunity to make our own scientific observations with the KING telescope of the MPIA. For that, we first had to choose an object to observe. This was done with the help of our tutor Sarah Leslie. We decided to observe the galaxy M81 in the constellation Ursa Major. We began our observation by taking sky flats and then waited until we could see the stars to proceed. We then proceeded by trying to find the right position, as the control board of the telescope doesn't show the right coordinates. To find out, where exactly the telescope is pointing, we had to use external software. During the observation, another problem became apparent: it was the night of a full moon and it was not that far away from out object. Additionally, it became cloudy after a short amount of time, so that we were only able to get pictures with two filters. You can see the resulting images, which we also performed bias and flat-field corrections upon, in figure 8.

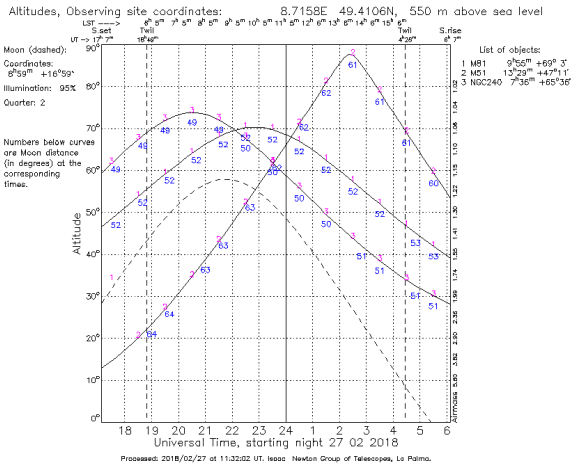

Figure 7: Apparent altitudes of different objects; preparation for observation

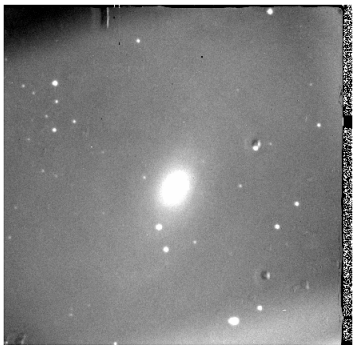

(a) R-band

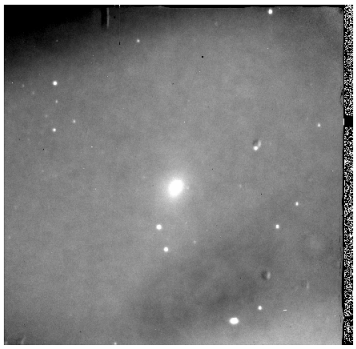

(b) V-band

Figure 8: Observation of M81 in R- and V-band

4 Discussion and summary

To summarise, we first familiarised ourselves with the bias-correction and then confirmed the temperature dependency of the dark current, given by Fermi statistics. From the plot(see fig.1) we deduced a band gap of $E_g = (1.202 \pm 0.006)eV$, which significantly deviates from the literature value for silicon $E_{g,SI} = 1.15eV$. We explained this by the fact that our detector is not made out of pure silicon, but rather a doped version. It can also have unintentional errors in its lattice as well as possible abrasion of its surface that comes from ageing.
In the next step, we created master flat-fields for different filters, which we used on different occasions, including a test run on a flat-field as seen in figure 3 which shows that it works well.
Next we confirmed a highly linear dependency of the measured signal from the integration time, as seen in figure 4. The linearity goes up to a flux corresponding to around 60,000 counts, after which saturation starts to set in.
Following that, we analysed the noise properties of the detector and found, that for a signal of around 30,000 counts, the photon noise slightly dominates over the PRNU noise, while the read-out noise is weaker by a factor of 2. Plotting the signal versus the noise revealed an irregular behaviour which

gave us two different gains κ, one for low and one for high counts, while deducing it from another formula gave us a third value: We explained this discrepancy by the fact that equation (8) can not

	κ
From plot using eq. (8)	940 ± 60
	-3540 ± 250
Using eq. (5)	230.30 ± 0.13

Table 2: Comparison of different gains κ

represent the whole relationship and by the fact that we used data from a point between the two κ to determine the third.

In the next part of the experiment, we computed a CMD of the globular cluster BS90 and manually fitted it with isochrones to determine its properties. From that, we got the following results: Those

	age [Gyr]	metallicity Z	distance d [kpc]
experiment	4.5 ± 0.1	$(1.5 \pm 0.5) \cdot 10^{-3}$	56.2 ± 2.6
literature [3]	4.5 ± 0.1	$(4 \pm 1) \cdot 10^{-3}$	58.9 ± 0.45

Table 3: Comparison of the BS90 measurements with literature

results overlap with the literature within 2σ, however, plotting the data from the literature seems to not match at all. This can be explained through a rather simple error on our side, as we had to use isolated stars from the image for calibration. However, only $4 \sim 5$ of the 10 stars used were actually isolated. The others had some overlap with other nearby stars. This slight error might be responsible for the deviation.

In the last part, we carried out our own observations of the galaxy M81. Unfortunately, we had several problems with the weather and moon conditions which resulted in rather unusable pictures.

5 References

[1] PhD students at the MPI for Astronomy.
FP30 CCD photometry in modern astronomy. Version 4.0.3, 10.08.2017

[2] SAGE Database. http://sage-doc.sis.uta.fi/reference/databases/

[3] B.Rochau, D.A.Gouliermis, W.Brandner, A.E.Dolphin, T.Henning.
The star-forming region NGC 346 in the small magellanic cloud with Hubble Space Telescope ACS observations. II. photometric study of the intermediate-age star cluster BS 90. arXiv:0704.2942 [astro-ph], 2007

[4] S. K. Yi, Y.-C. Kim, P. Demarque
The Y2 Stellar Evolutionary Tracks. ApJS, 144, 259, 2003